Inorg. Chem. **2004**, *43*, 8150–8157

Spin-Frustrated $(VO)_3^{6+}$-Triangle-Sandwiching Octadecatungstates as a New Class of Molecular Magnets

Toshihiro Yamase,*,† Eri Ishikawa,† Keisuke Fukaya,† Hiroyuki Nojiri,‡ Tomohiro Taniguchi,‡ and Tooru Atake§

Chemical Resources Laboratory, Tokyo Institute of Technology, R1-21, 4259 Nagatsuta, Midori-ku, Yokohama 226-8503, Japan, "Creation of bio-devices and bio-systems with chemical and biological molecules for medical use", CREST, Japan Science and Technology Agency (JST), Japan, Department of Physics, Okayama University, Tsushimanaka 3-1-1, Okayama 700-8530, Japan, and Materials and Structures Laboratory, Tokyo Institute of Technology, R3-7, 4259 Nagatsuta, Midori-ku, Yokohama 226-8503, Japan

Received March 15, 2004

Spin-frustrated polyoxometalates, $K_{11}H[(VO)_3(SbW_9O_{33})_2]\cdot 27H_2O$ (**1**) and $K_{12}[(VO)_3(BiW_9O_{33})_2]\cdot 29H_2O$ (**2**), containing approximately equilateral and isosceles $(VO)_3^{6+}$-triangles ($V^{IV}\cdots V^{IV}$ separation of 5.4–5.5 Å) sandwiched by two diamagnetic α-B nonatungstate ligands ($[SbW_9O_{33}]^{9-}$ and $[BiW_9O_{33}]^{9-}$) with approximate D_{3h} symmetry, are found to show magnetization jumps with distinct hysteresis for the $S = {}^1/_2 \leftrightarrow S = {}^3/_2$ level crossing under fast sweeping pulsed magnetic fields ($\sim 10^3$ T/s) at $T \leq 0.5$ K. This unusual phenomenon is attributed to the theoretical prediction of half step magnetization, which is expected for an antiferromagnetic spin triangle with antisymmetrical Dzyaloshinky–Moriya interaction. The degeneracy of the $S = {}^1/_2$ states for **1** is removed by slightly lower symmetry effects of triangular structure for **2**. The calorimetry of **1** and **2** shows the heat capacity anomaly at $2 \leq T \leq 20$ K which is associated with a thermal excitation from the $S = {}^1/_2$ ground states to the $S = {}^3/_2$ state at zero field. Zero-field splitting energies (5–7 K) between $S = {}^1/_2$ and $S = {}^3/_2$ states for **1** and **2**, readily estimated by the level-crossing field for the magnetization, allow us to measure the hyperfine-structural 22 lines due to three equivalent $I = {}^7/_2$ ^{51}V nuclei, the fine-structural triplet line of the $S = {}^3/_2$ excited state, and the g anisotropy on the high-frequency ESR spectra. The spin-frustrated $(VO)_3^{6+}$-triangle for **1** and **2** is a good model of the magnetization between pure quantum states $S = {}^1/_2$ and ${}^3/_2$ and provides a new class of single-molecule magnets.

Introduction

Polyoxometalates comprise a versatile class of inorganic, anionic clusters that has made a mark on disciplines as diverse as materials science involving electronic, magnetic, electrochemical, and photochemical properties, medicine as antitumor, antiviral, and antimicrobacterial agents, homogeneous and heterogeneous catalysts, and photocatalysts.[1] In the course of our work on application of polyoxometalates into medicine,[2] we recently found $(VO)_3^{6+}$-triangle-sandwiching polyoxotungstate $[(VO)_3(SbW_9O_{33})_2]^{12-}$ and its one-electron oxidation species $[(VO)_3(SbW_9O_{33})_2]^{11-}$ to exhibit a potent activity against a wide variety of the enveloped RNA viruses which infect high-risk individuals, such as infants born with prematurity, cardiovascular failure, pulmonary dysplasia, and immunodeficiency.[3] We have also investigated the physicochemical properties of $[(VO)_3(SbW_9O_{33})_2]^{12-}$ in relevance to its application into a new class of antiviral drugs.

* To whom correspondence should be addressed. E-mail: tyamase@res.titech.ac.jp. Phone: +81-45-924-5260. Fax: +81-45-924-5260.

† Tokyo Institute of Technology and CREST, Japan Science and Technology Agency (JST).

‡ Okayama University.

§ Tokyo Institute of Technology.

(1) (a) *Polyoxometallates: From Platonic Solids to Anti-Retroviral Activity*; Pope M. T., Müller A., Eds.; Kluwer Academic Publishers: New York, 1994. (b) Yamase, T. In *Polymeric Materials Encyclopedia: Synthesis, Properties, and Applications*; Salamone, J. C., Ed.; CRC Press: Boca Raton, FL, 1996; pp 365−373. (c) Hill, C. L., Ed. *Chem. Rev.* **1998**, *98*, 1−387. (d) *Polyoxometallates: From Topology to Industrial Applications*; Pope, M. T., Müller, A., Eds.; Kluwer Academic Publishers: New York, 2001. (e) *Polyoxometalate Chemistry for Nanocomposite Design*; Yamase, T., Pope, M. T., Eds.; Kluwer Academic/Plenum Publishers: New York, 2002. (e) *Polyoxometalate Molecular Science*; Borrás-Alamenar, J. J., Coronado, E., Müller, A., Pope, M. T., Eds.; NATO Science Series; Kluwer Academic Publishers: New York, 2003. (f) Yamase, T. *Catalysis Surv. Asia* **2003**, *7*, 203−217.

10.1021/ic049669n CCC: $27.50
Published on Web 11/13/2004

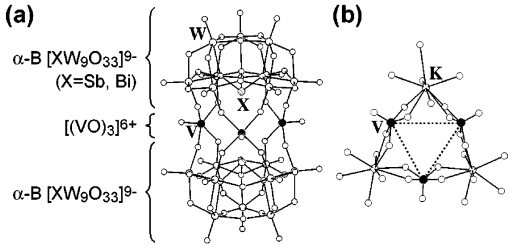

Figure 1. Structure (a) of $[(VO)_3(XW_9O_{33})_2]^{12-}$ (X = Sb^{III}, Bi^{III}) and the stabilization (b) of VO^{2+}-triangle by three K^+ cations in the equatorial V_3 plane. Open, shaded, striped, and filled circles represent O, V, Sb (or Bi), and K atoms, respectively: $V-O_{terminal}$ 1.56−1.60, $V-O_{bridge}$ 1.92−1.99, V···V 5.37−5.47, K···K 7.64−7.80, Sb(Bi)···Sb(Bi) 4.78(4.50) Å distances.

The anion structure of $[(VO)_3(XW_9O_{33})_2]^{12-}$ (X = Sb^{III} and Bi^{III}) for $K_{11}H[(VO)_3(SbW_9O_{33})_2]\cdot 27H_2O$ (**1**) and $K_{12}[(VO)_3(BiW_9O_{33})_2]\cdot 29H_2O$ (**2**) consists of a VO^{2+} (spin quantum number $S = {}^1/_2$ for each) triangular cluster (with $V^{IV}\cdots V^{IV}$ separation of 5.4−5.5 Å), sandwiched by two diamagnetic α-B $[XW_9O_{33}]^{9-}$ (X = Sb^{III} and Bi^{III}) ligands in D_{3h} of the local symmetry and stabilized by three equatorial K^+ ions linking three distorted VO_5 square-pyramids in alternate positions to form the six-membered ring with K···K distances of 7.64−7.80 Å (Figure 1).[4,5]

Compounds **1** and **2** provide simple models for understanding intramolecular spin−spin interactions between V^{IV} centers of the magnetically intriguing high-nuclearity-polyoxovanadates. If the magnetic interaction within the central $(VO)_3^{6+}$-triangle is antiferromagnetic, the resultant ground spin state at low temperatures becomes $S = {}^1/_2$. When the Heisenberg approach is valid, the three spins for the $(VO)_3^{6+}$-triangle can be coupled into a quartet ($S = {}^3/_2$) and two doublets ($S = {}^1/_2$). If three spins are at the corners of an isosceles triangle as for $[(VO)_3(BiW_9O_{33})_2]^{12-}$ (with V···V distances 5.38−5.48 Å), then the spin exchange Hamiltonian H is

$$\mathbf{H} = J(s_1\cdot s_2 + s_2\cdot s_3) + J_1(s_3\cdot s_1) \qquad (1)$$

where J and J_1 account for exchange interactions between the distorted square-pyramidal V^{IV} centers located inside $(VO)_3^{6+}$-triangle.[6] The energy level diagram places the quartet state at $J/2 + J_1/4$, one doublet at $-3J_1/4$, and the second doublet at $-J + J_1/4$. If three spins are located on the corners of an equilateral triangle as for $[(VO)_3(SbW_9O_{33})_2]^{12-}$ (with V···V distances 5.41−5.46 Å), J and J_1 are equal, and the quartet lies at $3J/4$ and the two doublets are degenerate at $-3J/4$. The zero-field splitting (Δ) between $S = {}^1/_2$ and $S = {}^3/_2$ states for the $(VO)_3^{6+}$-triangles presages the magnetization jump, when the magnetic field fulfills the condition of $B_c = \Delta/g\mu_B$ (B_c, g, and μ_B being level-crossing magnetic field, g-value, and the Bohr magneton) where two Zeeman splitting energy levels belonging to different spin magnetic quantum number (M_s) states coincide.[7,8] The spectroscopy of the magnetization step for measuring intracluster magnetic interactions has been established in the outstanding works in diluted semiconductors,[9] and some new aspect may be seen in a nanosize molecular magnet. Under equilibrium conditions, the magnetization curve of the system can be easily calculated by using the Boltzmann distribution function, and the jump from 1 to 3 μ_B is expected at the level crossing for the spin triangle. However, this is not necessarily valid for the magnetization curve at zero temperature limits, since magnetization is kept constant at level crossing, if there is no mixing between corresponding levels. In turn, an adiabatic change of magnetization is expected, when the mixing causes a tunneling gap. Such a purely quantum-mechanical magnetization process is scarcely observed because thermal relaxation cannot be suppressed sufficiently in real experiments. Moreover, there is no qualitative difference between equilibrium and nonequilibrium magnetization processes in many cases.

An antiferromagnetic spin triangle is special because the ground state is doubly degenerated for the spin chirality. When a Dzyaloshinky−Moriya (DM) interaction exists, only one of the doublets mixes with the excited state $S = {}^3/_2$. In this case, the magnetization curve is qualitatively different between equilibrium and nonequilibrium conditions. Namely, the existence of the nonmixing doublet results in the half step magnetization in zero temperature limits.

In this paper, it is shown that **1** and **2** are spin-frustrated compounds and give the magnetization behavior under fast sweeping pulsed magnetic field (~10^3 T/s) at nonequilibrium to involve the $S = {}^1/_2 \leftrightarrow S = {}^3/_2$ level crossing through the quantum tunneling demonstrated by the DM interaction. Although there have been many investigations of magnetic behavior for structurally similar spin Cu_3^{6+}-triangle compounds such as $[Cu_3(H_2O)_2(AsW_9O_{33})_2]^{12-}$,[6] $Cu_3(O_2C_{16}H_{23})_6$,[10] $[L_3Cu_3(im)_3]^{3-}$ (L = 1,4,7-trimethyl-1,4,7-triazacyclononane and im = imidazolate),[11] and $[Cu_3(cpse)_3(H_2O)_3]$ (cpse =

(2) (a) Yamase, T.; Tomita, K.; Seto, Y.; Fujita, H. In *Polymers in Medicine: Biomedical and Pharmaceutical Applications*; Technomic Publishing Company Inc.: Lancaster, PA, 1992; Chapter 13, pp 187−212. (b) Yamase, T. In *Molecular Engineering*; Kluwer Academic Publishers: New York, 1994; Vol. 3, pp 241−262. (c) Shigeta, S.; Mori, S.; Watanabe, J.; Soeda, S.; Takahashi, K.; Yamase, T. *Antimicrob. Agents Chemother*. **1997**, *41*, 1423−1427. (d) Fukuda, N.; Yamase, T. *Biol. Pharm. Bull*. **1997**, *20*, 927−930. (e) Fukuda, N.; Yamase, T.; Tajima, Y. *Biol. Pharm. Bull*. **1999**, *22*, 463−470. (f) Dan, K.; Miyashita, K.; Seto, Y.; Fujita, H.; Yamase, T. *Pharmacol. Res.* **2002**, *46*, 357−361.
(3) Shigeta, S.; Mori, S.; Kodama, E.; Kodama, J.; Takahashi, K.; Yamase, T. *Antiviral Res*. **2003**, *58*, 265−271.
(4) (a) Yamase, T.; Botar, B.; Ishikawa, E.; Fukaya, K. *Chem. Lett*. **2001**, 56−57. (b) Yamase, T.; Botar, B.; Ishikawa, E.; Fukaya, K.; Shigeta, S. In *Polyoxometalate Chemistry for Nanocomposite Design*; Yamase, T., Pope, M. T., Eds.; Kluwer Academic/Plenum Publishers: New York, 2002; pp 169−180.
(5) Botar, B.; Yamase, T.; Ishikawa, E. *Inorg. Chem. Commun*. **2001**, *4*, 551−554.
(6) Kokoszka, G. F.; Padula, F.; Goldstein, A. S.; Venturini, E. L.; Azevedo, L.; Siedle, A. R. *Inorg. Chem*. **1988**, *27*, 59−62.
(7) Friedman, J. R.; Sarachik, M. P.; Tejada, J.; Ziolo, R. *Phys. Rev. Lett*. **1996**, *76*, 3830−3833.
(8) Thomas, L.; Lionti, F.; Ballou, R.; Gatteschi, D.; Sessoli, R.; Barbara, B. *Nature* **1996**, *383*, 145−147.
(9) (a) Shapira, Y. *J. Appl. Phys.* **1990**, *67*, 5090−5095. (b) Shapira, Y.; Bindilatti, V. *J. Appl. Phys.* **2003**, *92*, 4155−4185. (c) Paduan-Filho, A.; Oliveira, N. F.; Bindilatti, V.; Foner, S.; Shapira, Y. *Phys. Rev. B*. **2003**, *68*, 3830−3833.
(10) Cage, B.; Cotton, F. A.; Dalal, N. S.; Hillard, E. A.; Rakvin, B.; Ramsey, C. M. *J. Am. Chem. Soc*. **2003**, *125*, 5270−5271.
(11) Padilla, J.; Gatteschi, D.; Chaudhuri, P. *Inorg. Chim. Acta* **1997**, *260*, 217−220.
(12) López-Sandoval, H.; Contreras, R.; Escuer, A.; Vicente, R.; Bernès, S.; Nöth, H.; Leigh, G. J.; Barba-Behrens, N. *J. Chem. Soc., Dalton Trans*. **2002**, 2548−2653.

doubly deprotonated form of *N*-[2-hydroxy-1(*S*)-methyl-2(*S*)-phenylethyl]-*N*-methyl glycine),[12] larger exchange interactions result in an experimental B_c-value that is too high (more than 230 T) for the level crossing with the $S = {}^3/_2$ state for the $Cu_3{}^{6+}$-triangle. The magnetization steps through quantum tunneling at the level crossing of $\Delta S = \pm 1$ have been investigated for many antiferromagnetic rings such as the ferric wheel, $[Fe_{10}(OMe)_2(CH_2ClCO_2)_{10}]$ (**Fe$_{10}$**), where no frustration is expected.[13] However, there are few examples of quantum tunneling for the frustrated spin ring in which three levels are involved in the level crossing for the spin chirality. As shown for the central $(VO)_3{}^{6+}$-triangle in a highly spin-abundant 15-VO^{2+} species, $K_6[V^{IV}{}_{15}As_6O_{42}(H_2O)]\cdot 8H_2O$ (**V$_{15}$**),[14] the magnetization of the degenerate $S = {}^1/_2$ ground states under the strong pulsed-magnetic field induces the jump of 1 μ_B at the level-crossing field,[15] different from the case (2 μ_B) of the equilibrium magnetization.[16] Such a half-step magnetization for **V$_{15}$** has been discussed in terms of the DM interaction which implies that only one of the $S = {}^1/_2$ doublets causes a tunneling gap at the level crossing with the $S = {}^3/_2$ state. In fact, the $(VO)_3{}^{6+}$-triangles allow the DM interaction due to the lack of inversion center, and the magnitude can be a few percent of the isotropic exchange coupling. The resultant gap can be much larger than those caused by other mechanisms such as dipolar interaction, single ion type anisotropy, and hyperfine interaction. Hence, the observation of pure quantum tunneling of magnetization at finite temperatures may be easier in the DM mechanism than in other mechanisms with a small tunneling gap. In **V$_{15}$**, however, the interaction path is complicated, and the modeling by a triangle might be too simple. The magnetization behavior of the $(VO)_3{}^{6+}$-triangles in **1** and **2** is interesting for their structural simplicity in relevance to the $(VO)_3{}^{6+}$-triangle compared to **V$_{15}$** consisting of a large number of spin states. Moreover, it is necessary to establish that the half-step magnetization is the essential and universal behavior of a triangular spin ring.

Experimental Section

$K_{11}H[(VO)_3(SbW_9O_{33})_2]\cdot 27H_2O$ (**1**) and $K_{12}[(VO)_3(BiW_9O_{33})_2]\cdot 29H_2O$ (**2**) were synthesized and purified by our previous method,[4,5] and $Na_9[SbW_9O_{33}]\cdot 19.5H_2O$ and $Na_9[BiW_9O_{33}]\cdot 16H_2O$ were synthesized by literature procedures.[17,18] All chemicals were of at least analytical grade and used without further purification. IR and UV−vis spectra were recorded on Jasco FT-IR 5000 and Jasco V-570 UV−vis−NIR spectrometers, respectively. The contents of K, V, Sb, W, and Bi were determined by X-ray fluorescence analysis on a JEOL JSX-3200 spectrometer. The water content was measured by thermogravimetric method on an ULVAC-TGD9600/MTS9000 instrument. X-band ESR measurements were carried out on a JEOL ESR spectrometer (JES-RE1X) equipped with a temperature-controlling unit (ES-DVT3) or an Oxford Instruments cryostat (ESR 910). The magnetic susceptibility in the range 4−300 K was measured under the magnetic field of 1.0 T with a Quantum Design MPMS-5S SQUID magnetometer, and the experimental data were corrected for diamagnetic contribution using standard Pascal constants.[19]

Heat capacity measurements were performed by a relaxation method using a Quantum Design PPMS in the temperature range from 2 to 20 K. A small amount of He gas was sealed in the calorimeter cell to aid the heat transfer. The amount of the sample used for the calorimetry was 14.78 and 7.68 mg for **1** and **2**, respectively. The heat capacity of the sample was obtained by subtracting the heat capacity of the calorimeter vessel from the total heat capacity. For determination of the excess heat capacities, we estimated a normal heat capacity curve or lattice heat capacity by the same manner as that described previously.[20]

Magnetization measurements were made by means of a standard inductive method.[21] A developed high-field system with variable sweep rate was designed by using a capacitor bank of variable capacitance (the maximum storing energies is 90 kJ). The apparatus for the pulsed magnetic-field generation was workable with high sweeping rates ($\sim 10^3$ T/s) using a ^{3}He refrigerator in the temperature range 0.3−20 K.[15a] The sample is immersed directly in the liquid of ^{3}He. Although the cryostat is heated by eddy current, the liquid evaporates slowly after each shot because of the low heat conduction between the wall of the cryostat and the sample specimen. The sample temperature is kept constant during field generation in many cases, which is confirmed by comparing with a magnetization curve measured in a cryostat made of plastic. It is notable that the effective temperature of the spin system can be different from the bath temperature in fast sweeping pulsed magnetic fields by the so-called magnetocaloric effect. The effect is very huge in molecular magnets because the intermolecular magnetic coupling is very weak. Gunn diodes were used as light sources for 110 and 130 GHz in ESR measurements under the high magnetic fields.

Results

Molar Heat Capacity. Molar magnetic susceptibility (χ) and temperature (T) products (χT) at 300 K for **1** and **2** (1.05 and 1.16 emu·mol^{-1} K) were close to the spin-only value (1.13 emu·mol^{-1} K) for the three V^{IV} centers, and the antiferromagnetic behavior for the χT plot against T strongly suggested the $S = {}^1/_2$ ground state of the molecules at low temperatures.[4] In order to investigate intracluster interactions, several sets of molar heat capacity (C_p) data for polycrystalline samples were obtained in the temperature range 2−20 K. C_p values of **1** and **2** under constant pressure at temperatures between 2 and 15 K are plotted in Figure 2a. A broad excess heat capacity (ΔC_p) anomaly, starting from

(13) Taft, K. L.; Delfs, C. D.; Papaefthymiou, G. C.; Foner, S.; Gatteschi, D.; Lippard, S. I. *J. Am. Chem. Soc.* **1994**, *116*, 823−832.
(14) (a) Müller, A.; Döring, J. *Angew. Chem., Int. Ed. Engl.* **1988**, *12*, 1721. (b) Müller, A.; Döring, J. *Z. Anorg. Allg. Chem.* **1991**, *595*, 251−274.
(15) (a) Nojiri, H.; Taniguchi, T.; Ajiro, Y.; Müller, A.; Barbara, B. *Physica B* **2004**, *346−347*, 216−220. (b) Miyashita, S.; Saito, K. *Physica B* **2003**, *329−333*, 1142−1143. (c) De Raedt, H.; Miyashita, S.; Michielsen, K. *Phys. Status Solidi B* **2004**, 1180−1185. (d) Chiorescu, I.; Wernsdorfer, W.; Müller, A.; Miyashita, S.; Barbara, B. *Phys. Rev.* **2003**, *B67*, 020402(R).
(16) Chiorescu, I.; Wernsdorfer, W.; Müller, A.; Bögge, H.; Barbara, B. *J. Magn. Magn. Mater.* **2000**, *221*, 103−109.
(17) Bösing, M.; Loose, I.; Pohlman, H.; Krebs, B. *Chem. Eur. J.* **1997**, *3*, 1232−1237.
(18) Botar, B.; Yamase, T.; Ishikawa, E. *Inorg. Chem. Commun.* **2000**, *3*, 579−584.
(19) O'Conner, C. J. *Prog. Inorg. Chem.* **1982**, *29*, 203−283.
(20) Morikawa, K.; Atake, T.; Wada, M.; Yamaguchi, T. *J. Phys. Soc. Jpn.* **1998**, *67*, 1994−1998.
(21) (a) Nakao, K.; Herlach, F.; Goto, T.; Takeyama, S.; Sakakibara, T.; Miura, N. *J. Phys. E: Sci. Instrum.* **1985**, *18*, 1018−1026. (b) Miura, N. *Physica B* **1994**, *201*, 40−48.

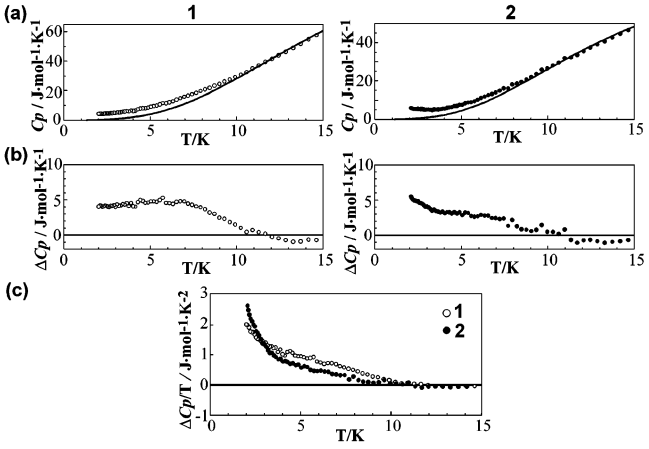

Figure 2. Molar heat capacities, C_p (a), excess heat capacities, ΔC_p (b), and excess entropies, $\Delta C_p/T$ (c), for **1** and **2**. The solid curves in part a show the estimated normal heat capacities.

~2 K, culminating at ~7 K, and terminating at ~11K, is observed (Figure 2b). The excess entropy gains determined by integration of ΔC_p with respect to ln T at $2 \leq T \leq 15$ K for **1** and **2** are 6.58 and 5.11 $J \cdot K^{-1} \cdot mol^{-1}$, respectively (Figure 2c). Figure 2c shows that the entropy gains at $T <$ 2 K remain with approximately equal magnitude and that the excess entropy gains for **1** and **2** at $0 < T < 15$ K are close to the value (R ln 4 = 11.52 $J \cdot K^{-1} \cdot mol^{-1}$, where R is molar gas constant) expected for the vibrational entropy change in the two spin-frustrated $S = {}^1/_2$ states (four magnetic levels) for **1** and **2**.

The crystal structure of **1** indicated disordering in 1 of 11 K^+ cations, in contrast to the one of **2** (showing no disordering in K^+ cations and solvated water molecules in lattice).[4,5] The result that the excess entropy gain at $0 < T < 15$ K for **1** is slightly larger than for **2**, therefore, may be elucidated by the contribution of the order−disorder transition in the K^+ cation.

Magnetic Hysteresis. Down to 0.5 K where the ground state will be the $S = {}^1/_2$ state and will consist of two degenerate doublet states, nonequilibrium behavior of the magnetization for **1** and **2** was observed at fast sweeping rates (~10^3 T/s) of the magnetic field. Results for **1** and **2** at 0.4 and 0.35 K, respectively, are shown in Figure 3a where the calculated magnetization curve (obtained by using the Boltzmann distribution function among two $S = {}^1/_2$ and one $S = {}^3/_2$ states with the measured level-crossing field and the averaged g value) at equilibrium for **1** is shown by the dotted line. When the field increases, the magnetization for **1** and **2** under the pulsed field at first approaches saturation around one Bohr magneton (μ_B), jumps around the $S = {}^1/_2 \rightarrow S = {}^3/_2$ level-crossing fields (B_c), and gradually increases to 3 μ_B (for **1**) and 2.5 μ_B (for **2**) in higher fields. The down sweep after saturation leads to hysteresis at both parts centered around B_c, which is peculiar for the VO^{2+} ion with a small anisotropy. The magnetization at low fields is smaller than that at equilibrium, as the field increases from 0 T (Figure 3a for **1**) to 2 T. This clearly indicates that the relaxation time between the $S_z = +{}^1/_2$ (upper) and the $S_z = -{}^1/_2$ (lower) is longer than the sweep period (about 10^{-3} s) of the field

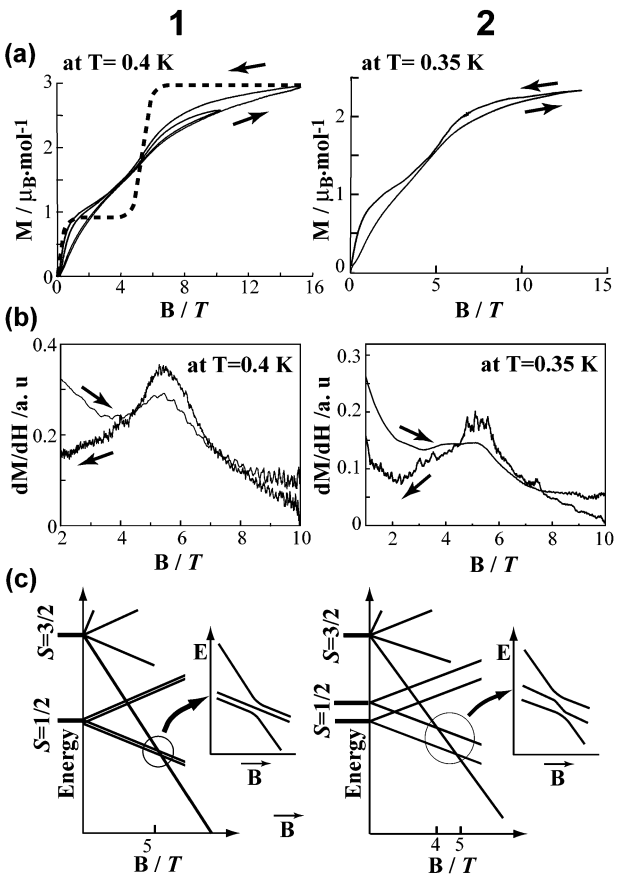

Figure 3. Magnetization (a) and differential magnetization (b) curves and energy-level diagrams for the level crossing (c) for **1** and **2**. Arrows indicate sweep directions. Open circles in part c indicate energy structures around the $S = {}^1/_2 \rightarrow S = {}^3/_2$ level-crossing field.

from 0 T up to 1 T. Starting from the equal population at zero field, the slow relaxation results in the excess population of the $S_z = +{}^1/_2$ state. In this condition, the decoupling (nonequilibrium) occurs between the spin system and the phonon bath. In other words, thermal relaxation is quenched by the fast sweeping pulsed field, which allows us to observe nonequilibrium behavior of the magnetization. Similarly, the hysteresis observed at high fields reflects the magnetization behavior of the $S = {}^1/_2 \leftrightarrow S = {}^3/_2$ level crossing which does not equilibrate, as discussed below. In the up sweep, the magnetization for **1** jumps to less than 2 μ_B from 1μ_B, and in the down sweep after saturation to 3μ_B the magnetization jumps down to around 1 μ_B. This behavior is similar to the magnetization of $\mathbf{V_{15}}$, which is the first example of such hysteresis.[15] The broader magnetization curves in the present experiments are partly due to the use of powder samples. In both present and previous cases, we infer that the major reason for the broadening is the large tunneling gap and the resultant significant bending of the levels around the level crossing, which are caused by the DM interaction. To see the hysteresis of jump more clearly, the differential magnetization (dM/dB) curves against the magnetic field for **1** and **2** are shown in Figure 3b. They show prominent peaks near the $S = {}^1/_2 \leftrightarrow S = {}^3/_2$ level-crossing fields with a pronounced hysteresis and stand out more clearly in the down traces (decreasing B) than in the up trace (increasing B). It is

noteworty that the widths of the peaks, which are sensitive to temperature, are nearly the same between the up and down sweeps. This indicates that the hysteresis in not caused by the change of spin temperature. Besides the common hystersis behavior, one important difference is observed between **1** and **2**. Namely, **1** exhibits a broad peak near 5.5 T, and for **2**, a shoulder peak near 4 T and a broad peak near 5.1 T are present. The additional magnetization jump near 4 T results from the isosceles triangle of $(VO)_3^{6+}$ for **2** in which the degeneracy of the two doublets would be removed into two separate $S = {}^1/_2$ states. The shoulder peak for the dM/dB curves corresponds to lower spin population at the upper $S = {}^1/_2$ state based on the Boltzmann distribution than at the lowest $S = {}^1/_2$ state. Figure 3c shows the energy diagrams of the level crossing for **1** and **2** in the existence of the DM interaction.

Thus, the $S = {}^1/_2 \leftrightarrow S = {}^3/_2$ level-crossing field (B_c = 5.5 T) for the approximately equilateral $(VO)_3^{6+}$-triangle in **1** indicates the doubly degenerate $S = {}^1/_2$ ground states with the zero-field splitting (Δ) $\approx$ 5.0 cm^{-1} (=7.2 K) to the $S = {}^3/_2$ excited state, and allows us to estimate the isotropic antiferromagnetic interaction (J_0) of the $S = {}^1/_2$ ground state to be J_0/hc = 3.3 cm^{-1} (J_0/k_B = 4.8 K) according to $3J_0/(2g\mu_B) = 5.5$ where the g value (=1.95) is assumed for **1** and **2**. Similarly, two separated $S = {}^1/_2$ states for the isosceles VO^{2+}-triangle in **2**, showing $B_c \approx 5$ and 4 T, are located with $J_0/hc \approx 3.0$ cm^{-1} (J_0/k_B = 4.4 K) and 2.1 cm^{-1} (=3.1 K), on $\Delta \approx 4.6$ cm^{-1} (=6.6 K) and 3.6 cm^{-1} (=5.2 K) to the $S = {}^3/_2$ excited state.

ESR Spectra. A multiline pattern due to the hyperfine interaction ($A_V \approx 3.2 \times 10^{-3}$ cm^{-1} = 4.6 mK) with three equivalent $I = {}^7/_2$ ^{51}V nuclei, partially buried in a broad singletlike isotropic signal at $g \approx 1.94$ ($\Delta H_{pp} \approx 34$ mT), was observed for the aqueous solutions of **1** and **2** at high temperatures of $T > 280$ K, as exemplified by the X-band ESR spectrum (Figure 4a) of **1** (11.3 mM) dissolved in water at 300 K. The signal intensity increased with an increase in the temperature with an accompanying development of line-resolution (for 22 lines) to the intensity ratio of approximately 1:3:6:10:15:21:28:36:42:46:48:48:46:42:36:28:21:15:10:6:3:1 (average line width of ~1.7 mT) at 350 K (Figure 4b). The 22-line ESR signal supports retention of the triangle nature of $(VO)_3^{6+}$ with almost equal possibility for each vertex of the triangle on dissolution in H_2O. When the solution is cooled to 273 K, the ESR signal progressively broadens and the hyperfine structure is lost. The singletlike ill-resolved broad lines (with half-width of ~40 mT) at $g \approx$ 1.95 were also observed for polycrystalline samples at the range 1.5−300 K. The 1.5-K ESR spectra of **1** for the frozen aqueous solution and the polycrystalline sample are shown in Figure 4c,d, respectively, where ill-resolved hyperfine structures from the multi-^{51}V nuclei coexist and prevent any conclusions concerning the possibility of localization of the electron on a single V atom.

The feature seems to be in a strong contrast with the occurrence of a Jahn−Teller distortion for the spin-frustrated Cu_3^{6+}-triangle compounds at very low temperature (4 K) where the unpaired electron orbital localizes on only one of the three nuclei of the Cu_3 trimer to result in observation of only four hyperfine lines due to the interaction with the $I = {}^3/_2$ Cu nucleus.[10,22]

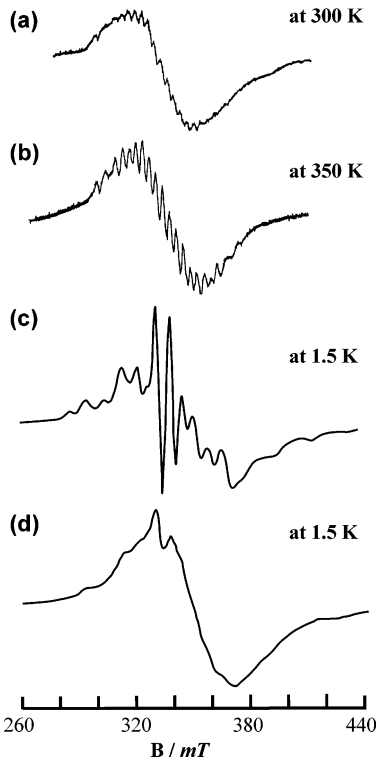

Figure 4. X-band solution and polycrystalline ESR spectra of **1**: 11.3 mM at 300 K (a), 350 K (b), and 1.5 K (c) in water, and polycrystalline at 1.5 K (d).

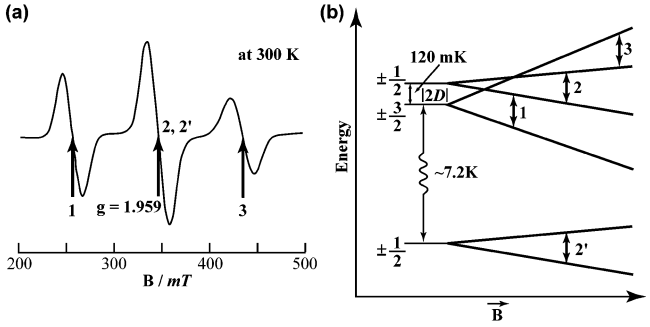

Figure 5. X-band single crystal (with $2 \times 4 \times 4$ mm^3 size) ESR spectrum for **1** at 300 K under the orientation of magnetic field with the z-direction of the axial symmetric paramagnet (a) and energy level diagram and expected ESR transitions (b).

The fine structure for the $S = {}^3/_2$ excited state derived from the exchange interaction was demonstrated by a single-crystal X-band ESR spectrum of **1** at room temperature. As shown in Figure 5a, three broad triplet lines appear at 255, 344, and 433 mT with equal separation of 89 mT under the orientation of magnetic field with the z-direction (along the $(VO)_3^{6+}$-triangle's 3-fold axis). The peak separation follows a (3 cos^2 θ−1) trend, where $\theta = 0°$ corresponds to the 3-fold symmetry axis. Thus, the energy splitting ($|2D|$) between Kramers doublets $S_z = \pm{}^3/_2$ and $S_z = \pm{}^1/_2$ for the $S = {}^3/_2$

(22) Angaridis, P. A.; Baran, P.; Boča, R.; Cervantes-Lee, F.; Haase, W.; Mezei, G.; Raptis, R. G.; Werner, R. *Inorg. Chem.* **2002**, *41*, 2219−2228.

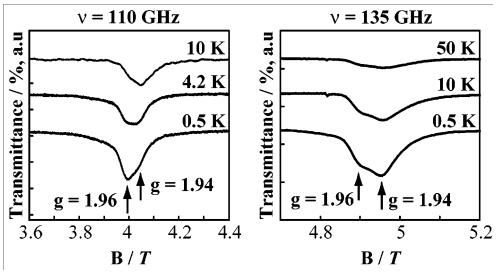

Figure 6. Temperature dependence of ESR spectra around the $S = {}^1/_2 \rightarrow S = {}^3/_2$ level-crossing field by a use of 110 and 135 GHz frequencies.

state, corresponding to the fine structure parameter (D), is $2D = -4.15 \times 10^{-2}$ cm^{-1} ($=-120$ mK). The negative sign on D was deduced from the observation that the highest field peak was always weaker than that at the lowest field, implying that in the $S = {}^3/_2$ state the $M_s = \pm{}^3/_2$ states lie lower than the $M_s = \pm{}^1/_2$ states (Figure 5b).[10]

The g value ($=1.959$) for the central line (corresponding to the $M_s = -{}^1/_2 \rightarrow M_s = +{}^1/_2$ transition) is close to the one estimated for the solution. The central component of the triplet is more intense than the outer peaks due to the fact that the ESR transition from the $S = {}^1/_2$ ground states occurs at the same field as shown in Figure 5b where the Δ-value estimated on the basis of the $S = {}^1/_2 \leftrightarrow S = {}^3/_2$ level-crossing field is notified. Although the detailed analysis of the single crystal X-band ESR spectra for **1** will be discussed in another paper, it is noteworthy to point out that the fine structure of the $S = {}^3/_2$ excited state observed at room temperature originates from the anisotropic exchange interaction ($J_z \neq J_x \approx J_y$) in the $(VO)_3{}^{6+}$-triangle, not from the a single ion type anisotropy being absent for $S = {}^1/_2$ spin. By considering both the exchange interaction and the Zeeman interaction under $g_x = g_y = g_z = 1.959$ for simplicity, the preliminary analysis of the room temperature single crystal ESR spectra of **1** results in $J_x/hc = 3.00$ cm^{-1} and $|J_{z-} - J_x|/hc = 0.17$ cm^{-1}, which indicates the anisotropy of approximately 6% for the exchange interaction within the $(VO)_3{}^{6+}$-triangle. The result is close to the isotropic antiferromagnetic J_0 value estimated from eq 1 using the above Δ-value obtained by B_c value, if $J_{z-} - J_x$ is positive.

The ground state of the spin-frustrated $(VO)_3{}^{6+}$-triangle cluster is changed from the $S = {}^1/_2$ to the $S = {}^3/_2$ at the level-crossing field (B_c) when the magnetic field increases (Figure 3c). Figure 6 shows temperature dependences of ESR spectra of the polycrystalline of **1** around B_c by the use of two kinds of frequencies, 110 and 135 GHz.

Two broad lines at $g = 1.96$ and 1.94 possibly reflect the quasiaxial symmetry of the g-value, which is consistent with the quasi-C_3 symmetery of crystals. The weak anisotropy within the plane normal to the quasi-C_3 axis could not be seen probably for the powder average. The g-value anisotropy is separated on the high-frequency ESR spectra, while the X-band ESR spectra did not give any g-separation due to unresolved broadening arising from the presence of the zero-field splitting between the $S = {}^1/_2$ and ${}^3/_2$ states. Similarly, two broad lines on 110- and 135-GHz ESR spectra were observed for **2**. The intensity of the $g = 1.94$ signal for 135 GHz (near B_c) is always high in the variety of temperature compared to that of the $g = 1.96$ signal. For 110 GHz, however, the relative intensity for the $g = 1.94$ signal decreases with decreasing temperature and becomes less at 0.5 K than for the $g = 1.96$ signal. This behavior may be related to the change of the ground state at the level crossing. The detailed analysis remains for further investigations.

Discussion

The ΔC_p anomaly took place within a narrow temperature range $\sim$11 K and showed a maximum around 7 K (Figure 2b). The culminating temperature roughly corresponds to the temperature at which the $S = {}^1/_2$ and the $S = {}^3/_2$ state distributions are equal, and the heat capacity hump is associated with the $S = {}^1/_2 \rightarrow S = {}^3/_2$ thermal excitation phenomenon. Although the measurement of the ΔC_p anomaly at temperatures $T \leq 2$ K was experimentally difficult, we can expect maxima of the excess entropy at nearly 1 K due to degenerate $S = {}^1/_2$ states for **1** and two separate $S = {}^1/_2$ states for **2**. The χT plots against T for **1** and **2** showed 1.05 and 1.16 emu·mol^{-1} K, respectively, which were close to the spin-only value (1.13 emu·mol^{-1} K) for the three V^{IV} centers in the $(VO)_3{}^{6+}$-triangle.[4] Thus, it is reasonable to discuss the exchange interaction of the $(VO)_3{}^{6+}$-triangle based on the Heisenberg spin-Hamiltonian by eq 1 without involving the orbital angular momentum. The J_0 value estimated by fitting χ data to the theoretical expression of χ is very small and almost the same ($J_0/hc = 1.4$ cm^{-1}, $J_0/k_B = 2.0$ K) for **1** and **2**.[4] On the other hand, the structural modification of the $(VO)_3{}^{6+}$-triangle was reflected by the level-crossing field in the magnetization, and its measurement under the fast sweep of the pulsed field gives us a great utility for estimating J_0 values of **1** and **2** (Figure 3).

Various studies on quantum tunneling have been performed so far with high-spin molecules such as $[Mn_{12}O_{12}(O_2CMe)_{16}(H_2O)_4]\cdot 2MeCO_2H\cdot H_2O$ (**Mn_{12}Ac**) and $[Fe_8O_2(OH)_{12}(tacn)_6]Br_8\cdot 9H_2O$ (**Fe_8**).[23] Especially, **Mn_{12}Ac** is a small ferromagnet, and tunneling occurs between two states separated by the anisotropy barrier with a resultant magnetic hysteresis. In such high-spin molecules, the tunneling gap at the level crossing is usually so small that the effect of nuclear dipolar moments is not negligible, and such a mixing of various electronic terms into the spin state makes it difficult to observe pure quantum tunneling. In the low-spin systems ($S = {}^1/_2$ state) with antiferromagnetic $(VO)_3{}^{6+}$-triangle spin networks for **1** and **2**, on the other hand, the metastable states separated by the anisotropy barrier do not exist because of the absence of the single-ion anisotropy. Interestingly, nevertheless, **1** and **2** in fast sweeping of the magnetic field show the hysteresis at magnetization jump due to the nonequilibrium of spin populations between the two degenerated spin chiral states (Figure 3a).

The importance of spin chirality was first pointed out for the magnetization reversal of **V_{15}** molecule at zero field.[15,16,24]

(23) (a) Gunther, L.; Barbara, B. *Quantum Tunneling of Magnetization*; Kluwer Academic Publishers: New York, 1995. (b) Thomas, L.; Lionti, F.; Ballou, R.; Gatteschi, D.; Sessoli, R.; Barbara, B. *Nature* **1996**, *383*, 145−147. (c) Barra, A. L.; Debrunner, P.; Gatteschi, D.; Schulz, C. E.; Sessoli, R. *Europhys. Lett.* **1996**, *35*, 133−138. (d) Gatteschi, D.; Sessoli, R. *Angew. Chem., Int. Ed.* **2003**, *42*, 268−297.

As is well-known, the zero-field gap is forbidden in a single $S = {}^1/_2$ doublet for time reversal symmetry, and thus, there should be no mixing between $S_z = +{}^1/_2$ and $S_z = -{}^1/_2$ states. In this case, the high sweeping rate compared to the relaxation time between $S_z = \pm{}^1/_2$ induces the hysteresis based on the nonequilibrium of the spin population in two $S_z = \pm{}^1/_2$ states. In the $\mathbf{V_{15}}$ molecule, it is found that the magnetization smoothly reverses at zero fields even at very low temperatures. It indicates that the magnetization is adiabatic, and there is a zero-field gap separating the ground state energy level from the excited state energy level. In the $(VO)_3{}^{6+}$-triangle system showing two degenerate $S = {}^1/_2$ ground states with relevance of spin chirality at zero-field, however, some types of perturbational interactions cause the avoided level crossing structure at zero field. It does not contradict with the time reversal symmetry because the double degeneracy is kept for the two branches with different chirality. In other words, the zero-field gap can open between the two sets of doubly degenerated states.[16,24] It has been theoretically proposed that the origin of this interesting tunneling-gap at zero-field is the DM interaction.[25]

It is predicted that the involvement of the DM interaction results in the formation of a tunneling-gap in only one chiral branch of the $S = {}^1/_2$ state at the level crossing with the $S = {}^3/_2$ state. This would give an adiabatic transition to the $S = {}^3/_2$ state at the field. No tunneling-gap in the other chiral branch results in the absence of magnetization jump in zero temperature limits. This special level-crossing nature causes a half step of magnetization. In the magnetization curve measured in steady magnetic field, no indication of such half step magnetization was observed. When the pulsed magnetic fields were swept as fast as the relaxation time, the half step feature is observed at the $S = {}^1/_2 \rightarrow S = {}^3/_2$ level crossing.[15] Unfortunately, $\mathbf{V_{15}}$ is not a simple $(VO)_3{}^{6+}$-triangle species:[14,26] It comprises 15 VO^{2+} groups, with a structure made up of three metal-ion layers containing hexagonal six, triangular three, and hexagonal six vanadium(IV) ions, respectively, where a spin of the inner V_3 triangle connects to the spins of the upper and lower V_6 hexagons. From this structure, it is inferred that the exchange coupling among three VO^{2+} spins in the $(VO)_3{}^{6+}$-triangle is mediated by the V^{IV} ions in two hexagons. It is very difficult to apply a simple triangle spin model for $\mathbf{V_{15}}$. From this point, the magnetization for a simple $(VO)_3{}^{6+}$-triangle species of **1** makes much more sense whether the DM mechanism is operative in the spin−spin communication in the spin-frustrated $(VO)_3{}^{6+}$-triangle species or not.

As shown in Figure 3b, two dM/dB curves against up and down sweeps for **1** or **2** show the same peak fields of B_c, and the magnetization jump for the down sweep is always higher than for the up sweep. These results strongly support the involvement of the DM-interaction induced half-magnetization at the $S = {}^1/_2 \rightarrow S = {}^3/_2$ level crossing. If the difference in the magnetization behavior between up and down sweeps is attributed to lowering of the effective spin temperature after saturated magnetization based on a decrease of the entropy of the spin system in these processes,[27] the peak width on the dM/dB curve should reflect this type of magnetization step. No observation of a significant difference in the peak widths against up and down sweeps on the dM/dB curves excludes this possibility.

In conjunction with the observation of nearly half magnetization in the up sweep, thus, it is clear that the above-mentioned theoretical picture is applicable for a spin triangle. It is found that the magnetization step at the $S = {}^1/_2 \rightarrow S = {}^3/_2$ level crossing for **1** is much broader than at the equilibrium (Figure 3a). It indicates that the large tunneling-gap arises from a large extent of mixing between the $S = {}^1/_2$ and $S = {}^3/_2$ states at level-crossing field. Since the present experiments have been made on simpler systems, it may be useful for further quantitative theoretical analysis. The magnetization hysteresis of **2** does not give the saturation at 3 μ_B, since the magnetization (toward 2.5 μ_B) around 15 T reflects a remaining spin-population at the $S = {}^1/_2$ state (Figure 3a). It indicates that the relaxation of $S = {}^1/_2 \rightarrow S = {}^3/_2$ is slower in **2**. The difference may be due to the difference of degeneracy between **1** and **2**. Another interesting point is that the spin in the upper $S = {}^1/_2$ state shows the re-entrant type magnetization step by following the energy level depicted in Figure 3c. The state once changes from $S = {}^1/_2$ to $S = {}^3/_2$ at the level crossing in the lower field side, and then, it changes again from $S = {}^3/_2$ to $S = {}^1/_2$ at the level crossing in the higher field side. If the state changes from $S = {}^1/_2$ to $S = {}^3/_2$ in both of $S = {}^1/_2$ branches, the magnetization would be 3 μ_B after the two successive transitions. The large reduction of the magnetization in **2** supports that the change of state as $S = {}^1/_2 \rightarrow S = {}^3/_2 \rightarrow S = {}^1/_2$ is realized in **2**. Such a negative magnetization step is caused by the adiabatic change of magnetization, which is realized experimentally by the quenching of thermal relaxation under fast sweeping magnetic fields.

As for $\mathbf{V_{15}}$, the B_c-value ($\approx$3.0 T) measured by the fast sweeping of the pulsed field at nonequilibrium was in good agreement with the one ($\approx$2.8 T) obtained by magnetization at the thermodynamic equilibrium:[15a,16] the coupling between the VO^{2+} ions in the two hexagonal V_6 layers (with V$\cdots$V distances 2.87 and 3.05 Å) is strongly antiferromagnetic ($J_0/k_B = 800$ K), and the spin-frustrated triangular V_3-middle layer shows a hysteresis loop at $T \leq 0.5$ K due to the $S = {}^1/_2 \leftrightarrow S = {}^3/_2$ level crossing. Zero-field splitting (Δ) between the $S = {}^1/_2$ and ${}^3/_2$ states, isotropic antiferromagnetic exchange-interaction (J_0), and $V^{IV}\cdots V^{IV}$ distances for the $(VO)_3{}^{6+}$-triangles of **1**, **2**, and $\mathbf{V_{15}}$ are summarized in Figure 7 where the energy splitting ($|2D|$) between Kramers doublets for the $S = {}^3/_2$ excited state (asymmetric exchange contribution) and the zero-field splitting (Δ_{DM}) due to the DM interaction (antisymmetric exchange contribution) are omitted

(24) (a) Chiorescu, I.; Wernsdorfer, W.; Müller, A.; Bögge, H.; Barbara, B. *Phys. Rev. Lett.* **2000**, *84*, 3454−3457. (b) Chiorescu, I.; Wernsdorfer, W.; Müller, A.; Miyashita, S.; Barbara, B. *Phys. Rev. Rapid Commun.* **2003**, *B67*, 020402(R). (c) Barbara, B. *J. Mol. Struct.* **2003**, *656*, 135−140.

(25) Miyashita, S.; Nagasawa, N. *Prog. Theor. Phys.* **2001**, *106*, 533−549.

(26) Gatteschi, D.; Pardi, L.; Barra, A. L.; Müller, A.; Döring, J. *Nature* **1991**, *354*, 463−465.

(27) Carlin, R. L. *Magnetochemistry*, Springer-Verlag: New York, 1986.

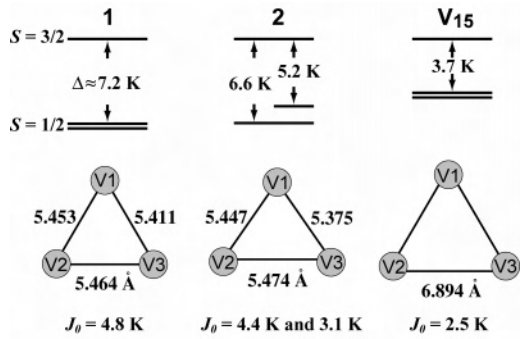

Figure 7. Isotropic antiferromagnetic exchange interaction (J_0) within $(VO)_3^{6+}$-triangles and zero-field splitting energy (Δ) between the $S = {}^1/_2$ and $S = {}^3/_2$ states for **1**, **2**, and $\mathbf{V_{15}}$. Zero-field splitting energies arising from antisymmetric exchange and asymmetric exchange contributions are omitted for their small values.

for their small value compared to Δ-value, as indicated by $|2D| = 120$ mK for **1** and $\Delta_{DM} \approx 50$ mK[16,24] for $\mathbf{V_{15}}$.

If one takes the extraordinarily long V···V distance of 6.89 Å for the $(VO)_3^{6+}$-triangle layer of $\mathbf{V_{15}}$ into consideration,[14] values $\Delta \approx 3.7$ K and $J_0/k_B \approx 2.5$ K for $\mathbf{V_{15}}$ are large enough to be expected from $\Delta = 7.2$ K and $J_0/k_B = 4.8$ K for nearly equilateral $(VO)_3^{6+}$-triangle (V···V distances 5.41−5.46 Å) in **1** and $\Delta = 6.6$ and 5.2 K and $J_0/k_B = 4.4$ and 3.1 K for the approximately isosceles $(VO)_3^{6+}$-triangle (V···V distances 5.38−5.48 Å) in **2**. The exchange interaction for the V_3 layer in $\mathbf{V_{15}}$ despite the long V···V distance of 6.89 Å has been explained by the perturbation terms arising from strong intramolecular antiferromagnetic interactions (in $J_0 \approx 150$ and 300 K) between the V_6 and V_3 layers (in V···V distances 3.02 and 3.73 Å).[16,26] It is noteworthy that the intermolecular shortest V···V distances for the $(VO)_3^{6+}$-triangle V atom are 5.523(2) and 5.835(2) Å from V_6-hexagon V atoms for the neighboring $\mathbf{V_{15}}$ molecule,[14] which suggest that the intermolecular exchange interaction for the V_3 layer of $\mathbf{V_{15}}$ is not negligible. In contrast, the shortest intermolecular V···V distances (7.934(8) and 7.910(5) Å) between the $(VO)_3^{6+}$-triangles for **1** and **2** are long enough to be isolated from intermolecular exchange interactions.

Finally, we would mention that the hysteresis for **1** and **2** is smaller than for $\mathbf{V_{15}}$ (Figure 3a).[15] This may be explained in terms of the relaxation time for magnetization which would be shorter for the former than for the latter, since the relaxation time will be governed by the $(VO)_3^{6+}$-triangle structure mainly associated with the $V^{IV}\cdots V^{IV}$ separation or the Hilbert-space dimension (2^3 in **1** and **2**, and 2^{15} in $\mathbf{V_{15}}$). Work on the magnetization both at much lower temperatures (near $T = 0$ K) and at shorter pulse field is necessary for the determination of the controlling factor of the relaxation time, where almost perfect half-step (with 1 μ_B) and full-step (with 2 μ_B) magnetizations at the $S = {}^1/_2 \rightarrow S = {}^3/_2$ level-crossing field would be observed for **1** and **2** (by assuming that the Boltzmann distribution for the upper $S = {}^1/_2$ state for **2** would be neglected at the temperature close to $T = 0$ K), respectively.

Acknowledgment. One (T.Y.) of us acknowledges Grants-in-Aid for Scientific Research, 14204067, from the Ministry of Education, Science, Sports, and Culture, and 99P01201 from RFTF/JSPS, and CREST of JST. H.N. acknowledges Grants-in-Aid for Scientific Research, from the Ministry of Education, Science, Sports, and Culture, and the support from Yamada Science Foundation. We thank Professor H. Takeuchi at the Toyota Institute of Technology for stimulating discussion on ESR spectra.

Note Added after ASAP Publication: The version of this paper published ASAP on November 13, 2004, contained an error in a formula in the last paragraph of the Introduction and a few inconsistencies in the notation for Tesla and temperature. The version published ASAP on November 18, 2004, has been corrected.

IC049669N